**Showcasing research from Grelet's group at Centre de Recherche Paul-Pascal, CNRS, University of Bordeaux, Pessac, France.**

Light-activated self-thermophoretic Janus nanopropellers

This study, led by Pr. Eric Grelet and colleagues, reveals how gold-silica (Au-SiO$_2$) Janus nanoparticles exhibit fuel-free, reversible self-thermophoretic motion under optical excitation. By carefully disentangling active dynamics from hot Brownian motion, this work provides direct experimental evidence of light-driven propulsion at the nanoscale, establishing a minimal photothermal system to explore fundamental non-equilibrium behaviors and active matter in 3D environments.

Image reproduced by permission of Henri Truong from *Nanoscale*, 2026, **18**, 5221.

As featured in:
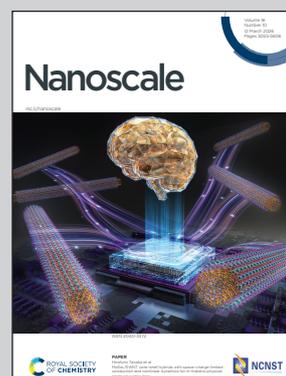
See Henri Truong *et al.*, *Nanoscale*, 2026, **18**, 5221.

ROYAL SOCIETY OF **CHEMISTRY**

rsc.li/nanoscale

Light-activated self-thermophoretic Janus nanopropellers

Henri Truong, [ID] [a] Chiara Moretti, [ID] [b] Lionel Buisson, [ID] [a] Benjamin Abécassis [ID] [b] and Eric Grelet [ID] *[a]

Achieving controlled and directed motion of artificial nanoscale systems in three-dimensional fluid environments remains a key-challenge in active matter, primarily due to the prevailing thermal fluctuations that rapidly randomize the particle trajectories. While significant progress has been made with micrometer-sized particles, imparting sufficient mechanical energy, or self-propulsion, to nanometer-sized particles to overcome Brownian diffusion and enable controlled transport remains a major issue for emerging applications in nanoscience and nanomedicine. Here, we address this challenge by demonstrating the fuel-free, reversible, and tunable active behavior of gold–silica (Au–SiO$_2$) Janus nanoparticles (radius $R \sim 33$ nm) induced by optical excitation. Using single particle tracking, we provide direct experimental evidence of self-thermophoresis, clearly distinguishing active motion from thermal noise. These light-driven Janus nanoparticles constitute a minimal yet robust photothermal system for investigating active matter and its manipulation at the nanoscale.

Introduction

Active Brownian matter, which converts external energy into autonomous motion at micro- and nanometric dimensions, provides unique opportunities to investigate nonequilibrium dynamics and develop functional devices at small scales. Natural examples such as motile bacteria and cytoskeletal filaments powered by motor proteins, illustrate how energy transduction can generate complex directed behavior.[1–5] Inspired by these biological systems, recent advances in nanotechnology have enabled the development of synthetic micro- and nanopropellers that harness chemical fuels, light, or electromagnetic fields to propel themselves through fluids.[6–9] While the controlled propulsion of micrometer-sized particles is now well established,[10] achieving reliable and tunable motion at the nanoscale remains a major challenge. At these dimensions, Brownian motion rapidly randomizes trajectories, hindering sustained directional transport in three-dimensional environments.[11] To design and characterize effective nanoscale propellers, it is therefore crucial to understand how random thermal fluctuations compete with and limit directed motion at these small scales.[12] Micro- and nanoparticles undergo passive Brownian motion described by their translational diffusion coefficient, $D_T = k_B T/6\pi\eta R$, and rotational diffusion coefficient, $D_R = k_B T/8\pi\eta R^3$, where R is the particle radius, k_B

the Boltzmann constant, T the absolute temperature, and η the solvent viscosity. As particle size decreases to the nanoscale, random thermal diffusion becomes stronger, counteracting any directed motion, while the propulsion efficiency typically decreases, as it is usually related to the particle surface area. To compare the effects of directed propulsion, with velocity v, to stochastic Brownian motion, the dimensionless Péclet number (Pe) is commonly used,[13] defined as $\mathrm{Pe} \propto \frac{v}{\sqrt{D_T \cdot D_R}}$.

When Pe ~ 1, active and passive contributions are comparable, making the clear demonstration and control of nanoscale propulsion particularly demanding. To address this challenge, various nanopropeller designs and actuation strategies have been proposed, tailored to specific applications such as targeted drug delivery, precision nanosurgery, biopsy, and related fields of nanomedicine.[14–22] Among these approaches, light-driven propulsion is particularly promising, as it enables fuel-free, reversible, and tunable control of nanoswimmer behavior.[23–33] Building on this concept, we demonstrate self-thermophoretic propulsion of gold–silica (Au–SiO$_2$) Janus nanoparticles under optical excitation. Our Janus particles, with a radius of $R \sim 33$ nm, consist of spherical gold cores partially coated with an asymmetric silica shell. Using single-particle tracking *via* optical microscopy, we provide direct experimental evidence that these visible-light-activated nanopropellers generate sufficient mechanical energy to overcome Brownian diffusion, with active and passive contributions to their dynamics being comparable (Pe ~ 1). To isolate these contributions, we analyze the motion of Janus nanoparticles relative to that of bare gold nanoparticles under identical con-

aUniv. Bordeaux, CNRS, Centre de Recherche Paul-Pascal (CRPP), UMR 5031, 115 Avenue Schweitzer, F-33600 Pessac, France. E-mail: eric.grelet@crpp.cnrs.fr
bCNRS, ENSL, Laboratoire de Chimie, UMR 5182, 46 allée d'Italie, F-69364 Lyon, France

ditions, enabling direct characterization and quantification of the tunable active self-propulsion, distinct from the passive component arising from hot Brownian motion. Our study establishes a minimal yet robust system for investigating and manipulating active matter at the nanoscale.

Materials and methods

Synthesis and characterization of Au–SiO$_2$ Janus nanoparticles

Gold–silica Janus nanoparticles are synthesized *via* selective silica (SiO$_2$) nucleation on one hemisphere of gold nanospheres.[34] The Janus morphology is confirmed by transmission electron microscopy (TEM), as shown in Fig. 1.
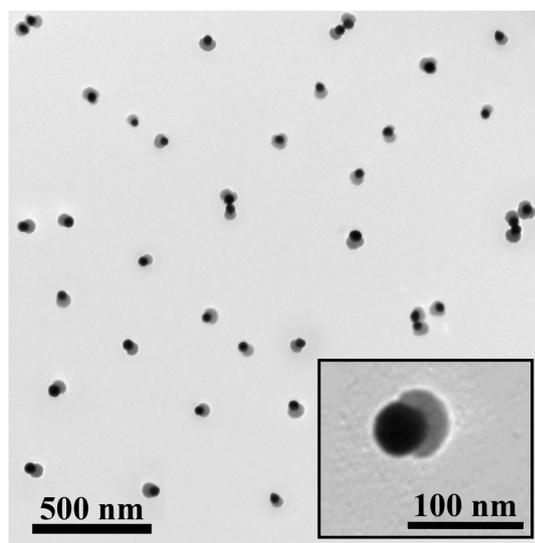

Fig. 1 Transmission electron microscopy (TEM) image of Au–SiO$_2$ Janus nanoparticles. The inset displays a high-magnification view of an individual Janus nanoparticle, revealing the distinct contrast between the silica shell (light gray) and the Au nanobead (black).

Specifically, the gold nanoparticles are synthesized using the multi-step protocol described by Bastús *et al.*[35] This results in gold nanobeads with an average diameter of d_{Au} = 40.3 ± 5.2 nm, as determined from the size distribution shown in Fig. 2(a). The selective growth of a silica shell on one hemisphere of the Au nanoparticles is performed following the procedure published by Chen *et al.*[36] and by Castro *et al.*,[34] using an alcohol/water solution as the reaction medium. Surface functionalization is achieved by grafting two competing ligands: polyacrylic acid (PAA) and 4-mercaptophenylacetic acid (MPAA). Due to their chemical incompatibility, these surfactants undergo phase separation, forming distinct patches of homogeneous composition on the nanoparticle surface. The subsequent addition of tetraethyl orthosilicate (TEOS) induces the selective nucleation of porous silica on the MPAA functionalized regions, resulting in the formation of Au–SiO$_2$ heterodimers. The silica shell has an average thickness of about 25 nm (Fig. 1), producing Janus nanoparticles with a major axis of d_{Janus} = 66.4 ± 7.2 nm (Fig. 2(b)), as determined by TEM. For TEM analysis, nanoparticles (~10^9 particles per mL), are deposited onto O$_2$ plasma-treated carbon-coated grids. Imaging is performed using a Hitachi H-600 electron microscope operating at 75 kV, equipped with an AMT CCD camera for image acquisition.

The visible light absorption spectra of both Janus and Au nanoparticle suspensions are recorded using a Nanodrop One spectrophotometer (Thermo Scientific) (Fig. 3), enabling concentration determination. The Janus nanoparticle suspension exhibits a red shift in the plasmon resonance peak from ~530 nm to ~540 nm. This shift is attributed not only to the growth of the silica shell, but also to changes in the local environment due to ligand exchange, notably the presence of thiol groups bound to the nanoparticle surface.[37] It is worth mentioning that nanoparticle suspensions exhibit excellent colloidal stability, with no observable aggregation over several months. Before thermophoresis experiments, suspensions are dialysed against a propionate buffer (pH 5.5, ionic strength I = 0.5 mM).
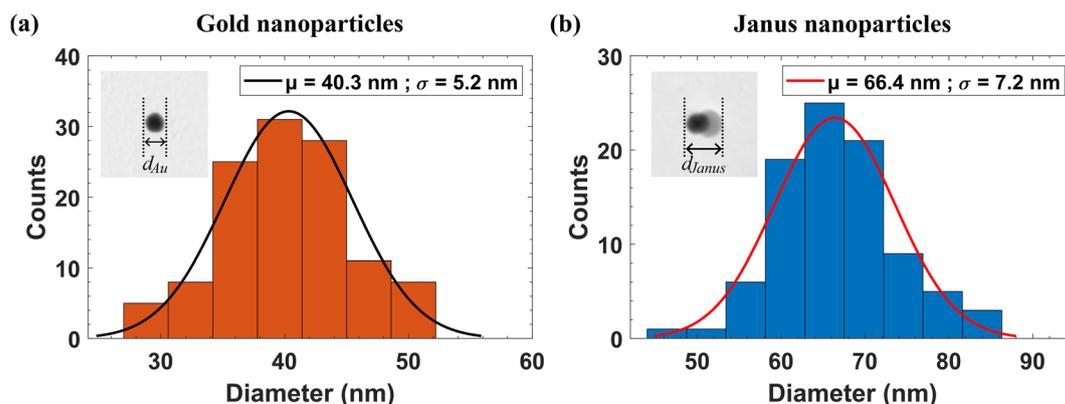

Fig. 2 Nanoparticle size distribution determined by transmission electron microscopy (TEM). (a) Bare gold nanobeads (*N* = 116) and (b) Janus nanoparticles (*N* = 90). The gold nanobeads are nearly spherical, characterized by a diameter d_{Au}, while d_{Janus} refers to the major axis of the Janus nanoparticles (see inset). Solid lines represent Gaussian fits to the measured size distributions; error bars on the particle diameter correspond to the standard deviation of these fits: d_{Au} = 40.3 ± 5.2 nm and d_{Janus} = 66.4 ± 7.2 nm.
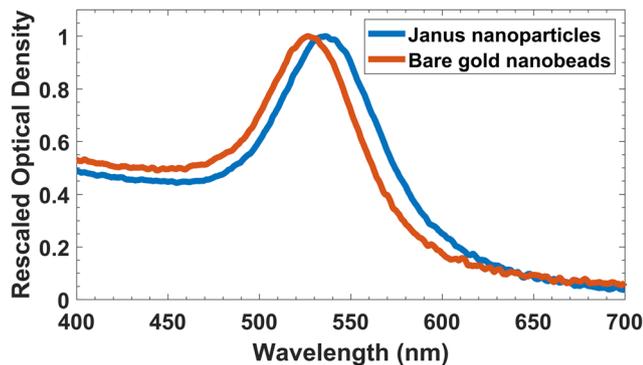
Fig. 3 Visible absorption spectra of Janus nanoparticles (blue line) and bare gold nanobeads (orange line). For comparison purposes, the optical density of each spectrum has been normalized to its respective maximum absorption value to account for the difference in sample concentration. The corresponding maximum optical densities are $OD_{max,Au}$ = 3.56 and $OD_{max,Janus}$ = 2.99.

Optical setup

The sample is visualized using a Dark-Field (DF) microscopy setup equipped with an Olympus UPlanFLN 100× oil immersion objective with an adjustable numerical aperture ($NA_{objective}$ = 0.6–1.3) and an Olympus U-DCW oil immersion dark-field condenser ($NA_{condenser}$ = 1.2–1.4). 1000 images per video are acquired using a Hamamatsu ORCA-Quest qCMOS camera C15550-20U at an effective pixel size of 2 × 4.6 μm (Binning 2) and a frame rate of 476 fps.

The optical excitation targeting an homogeneous illumination of the sample is carried out using a Spectra-physics Excelsior 532 Single Mode laser (λ = 532 nm, maximum nominal output power: 200 mW). To protect the camera from laser exposure, two notch filters are placed in the imaging path.

The incident laser power on the sample is measured and calibrated before each experimental session using a photodiode (Thorlabs S121C) positioned at the sample level. The laser power is modulated using a Glan–Thompson prism, acting as polarizer, paired with a rotating half-wave (λ/2) plate. The beam size is first increased using a Thorlabs GBE05-A 5× beam expander, and then further enlarged through a series of lenses (L1 and L2) to ensure full illumination of the objective's back focal plane (Fig. 4). To reduce light intensity gradient across the sample area, the final lens in the optical path is axially translated by a few millimeters (distance d_L in Fig. 4), generating controlled beam divergence before the back focal plane of the objective. This slight defocusing broadens the beam profile, thereby enhancing illumination uniformity, with an estimated beam size of about 130 μm. Under these conditions, no optical artifacts, including nanoparticle optical trapping, are detected, even at the maximum incident laser power of P = 81 mW on the sample (after accounting for optical losses in the setup).

Sample preparation and single particle tracking (SPT)

For thermophoresis experiments, the particle concentration is set in the dilute regime at $c \sim 3.6 \times 10^9$ particles per mL (OD_{520nm} = 0.05), as shown in Fig. 5. Microscope cells for imaging the samples are prepared by thoroughly cleaning glass slides and 0.17 mm-thick cover glasses (18 × 18 mm) with chromosulfuric acid to remove organic contaminants. Subsequently, both glass components are treated with an O_2 plasma cleaner (Basic Plasma Cleaner, Harrick Plasma) to enhance surface hydrophilicity. A 4 μL aliquot of the particle suspension is then deposited at the center of the glass slide, and the cover glass is gently placed on top of the droplet. The edges are immediately sealed with optical adhesive (Norland Optical Adhesive NOA 68), producing an observation chamber
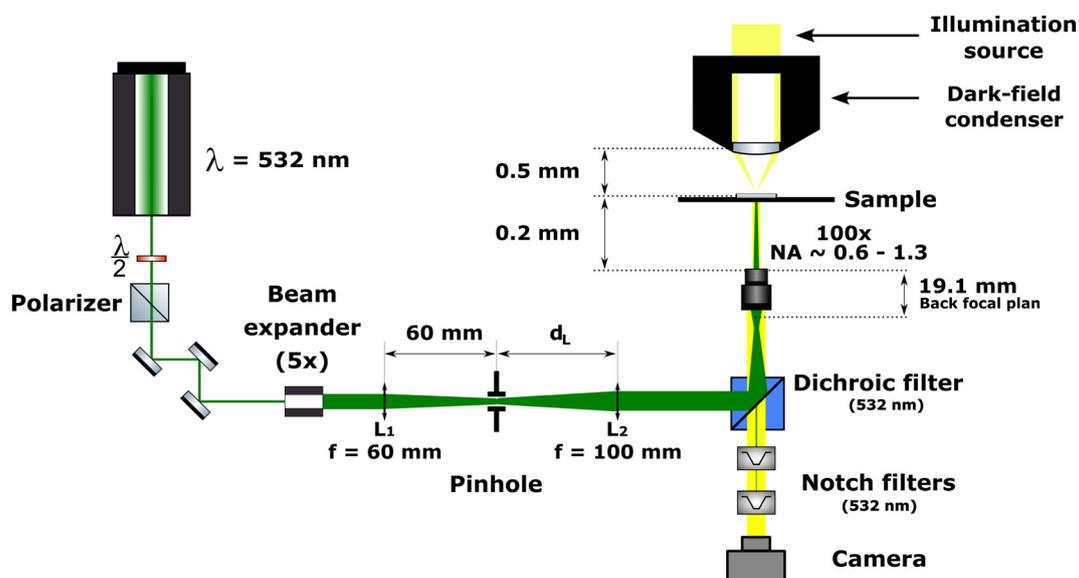
Fig. 4 Schematic representation of the optical setup enabling both direct visualization of the sample *via* dark-field microscopy and its excitation using green laser illumination.

Fig. 5 Dark-field microscopy image of the Janus nanoparticles. A representative frame acquired during the experiments (see Movie S1 in the SI), showing Janus nanoparticles in the absence of optical excitation. Although individual nanoparticles are subject to optical resolution limits, this does not prevent the precise determination of their center-of-mass position *via* single particle tracking (see Material and methods). The sample concentration is set in the dilute regime at $c \approx 3.6 \times 10^9$ particles per mL.

approximately 10 μm thick. The mean inter-particle distance is estimated as $\langle l \rangle \sim n^{-1/3}$, where $n = N/V$ is the particle number density, yielding $\langle l \rangle \sim 6$ μm at this concentration. Given the nanoparticle diameter, this corresponds to a mean inter-particle distance $\frac{\langle l \rangle}{d}$ of approximately 100 times the particle size. Under these conditions, no collective behavior is expected from a colloidal standpoint, and the measured diffusion coefficients are expected to match those at infinite dilution.

Image acquisition is performed at the middle height of the observation cell, maintaining a distance of approximately 5 μm away from all surfaces to minimize surface–particle interactions. An initial reference experiment is performed without laser irradiation, followed by measurements under laser illumination, and concluded with a final control experiment. Prior to each acquisition at a given laser intensity, the sample is illuminated for 5 min to reach thermal steady state. Two-dimensional particle trajectories $\mathbf{r}(t)$ are determined using a custom-written MATLAB (MathWorks) particle-tracking algorithm, adapted from the method developed by Crocker and Grier.[38] Although the nanoparticles are smaller than the optical resolution limit, their center-of-mass positions are localized with sub-diffraction precision by fitting their diffraction patterns with a 2D Gaussian function.[39] Particle dynamics is characterized by calculating their Mean Squared Displacements (MSD), at lag time τ, defined as $\mathrm{MSD}(\tau) = \langle [\mathbf{r}(\tau + t) - \mathbf{r}(t)]^2 \rangle_t$ where $\langle ... \rangle_t$ denotes the average over all start times t. The MSD is calculated for each trace, before being first averaged over the total number of detected particles (around one hundred per experiment, see SI) and subsequently fitted to determine the corresponding effective diffusion coefficients (Fig. 6 and Fig. S1 & S2).[40,41]

Results and discussion

A batch of gold–silica Janus nanoparticles with a nominal diameter of approximately 66 nm has been produced *via* selective silica (SiO$_2$) nucleation on one hemisphere of gold nanospheres (see Materials and methods for more details). Bare gold nanobeads serve as an experimental control system to isolate the active contribution of the Au–SiO$_2$ Janus nanoparticles under optical excitation.

Particle dynamics is investigated in the dilute regime using Single Particle Tracking (SPT). Our custom setup combines Dark-Field (DF) microscopy[11] – which leverages the strong scattering signal of gold for high-contrast visualization – with simultaneous optical excitation of the sample *via* a defocused green laser beam ($\lambda = 532$ nm) delivered through the same objective (Fig. 4 and Materials and methods). A representative DF image of the Janus nanoparticles is provided in Fig. 5. Illumination homogeneity is rigorously controlled to eliminate artifacts induced from light gradients (Fig. 6).

Particle trajectories are captured as two-dimensional (2D) projections within the microscope focal plane. Due to the finite depth of field of the objective, these 2D trajectories result from the projection of the particle's full three-dimensional (3D) motion.[38–40] Fig. 7 displays representative trajectories of Janus nanoparticles acquired at increasing levels of optical excitation power. The rapid rotational diffusion, characterized by the rotational diffusion coefficient D_R, reflects frequent reorientation events contributing to the stochastic nature of the trajectories (Fig. 7). For a quantitative analysis of the particle dynamics, we compute the ensemble-averaged Mean Squared Displacement (MSD) from approximately 100 individual traces acquired for each experimental condition (see Materials and methods and Fig. S1 and S2). The resulting MSDs are displayed in Fig. 8.

The diffusion of a nanoparticle whose internal temperature exceeds that of the surrounding solvent is referred to as Hot Brownian Motion (HBM).[25,42–44] The heat generated by the particle generates a radially symmetric thermal "halo" in the surrounding solvent, altering the local temperature and viscosity profiles around the particle and resulting in an apparent increase in both the rotational and translational diffusion coefficients. Despite its inherently non-equilibrium feature, the system can be described in a quasi-steady state (enabled by the separation of timescales between heat diffusion and particle motion) using equilibrium-like Stokes–Einstein relations with two distinct apparent temperatures and viscosities associated with the translational and rotational degrees of freedom, respectively.[45,46] For translational motion, the effective diffusion coefficient for a particle undergoing hot Brownian motion can then be written as:

$$D_{\mathrm{eff}}^{\mathrm{HBM}} = \frac{k_B T_{\mathrm{eff}}}{6\pi \eta_{\mathrm{eff}} R} \qquad (1)$$

where the effective temperature is given by $T_{\mathrm{eff}} \simeq T_0 \left(1 + \frac{5}{12} \Delta T \right)$ with ΔT the temperature difference between the particle surface and the bulk solvent at temperature T_0, and
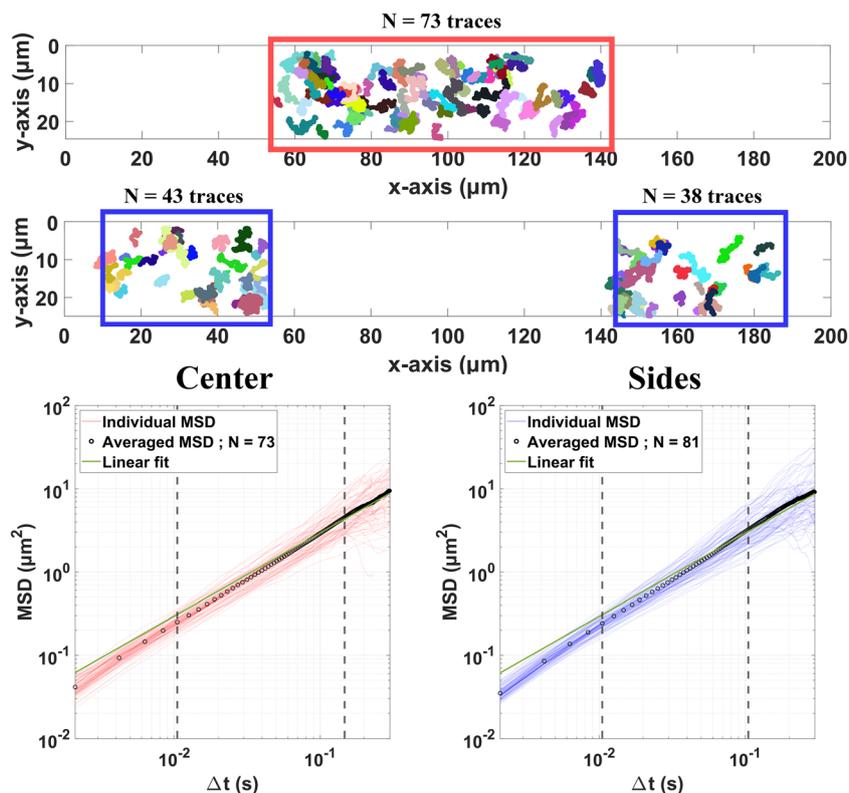
Fig. 6 Uniform illumination and Janus nanoparticle dynamics. Trajectories of Janus nanoparticles tracked using dark-field microscopy (see Fig. 5) under maximum laser illumination (P = 81 mW) are shown for particles located inside (red) and outside (blue) the central Region of Interest (ROI) (top and middle panels). The areas of the red and blue boxes are equal, resulting in similar numbers of traces (N = 73 for the central ROI and N = 81 [43 + 38] for the sides), allowing therefore a direct comparison of the dynamics. The corresponding mean squared displacement (MSD) curves are displayed (bottom panel), with red and blue curves corresponding to particles inside and outside the central ROI, respectively. Linear fits to the mean MSD curves yield diffusion coefficients of $D_{T,Center}$ = 7.31 μm^2 s^{-1} and $D_{T,Sides}$ = 7.26 μm^2 s^{-1}. The minimal difference between these values, which falls within the statistical error, confirms the spatial homogeneity of laser illumination across the field of view. Data represent averages over four independent acquisitions.
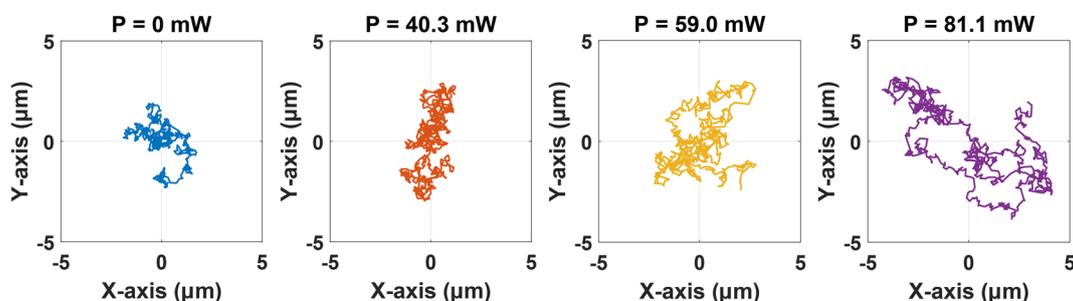

Fig. 7 Representative trajectories of Janus nanoparticles under increasing optical excitation power, illustrating the self-thermophoretic active contribution to their dynamics over a fixed trace duration of 1.8 s.

the analytical expression of the effective viscosity η_{eff} is provided in the SI (eqn (S4)).[42,43,46] The corresponding effective translational diffusion coefficient, D_{eff}^{HBM}, which depends on the laser-induced temperature increase ΔT, is related to the mean squared displacement in n dimensions and at a given lag time Δt by:

$$\mathrm{MSD}(\Delta t) = 2n D_{eff}^{HBM} \cdot \Delta t, \qquad (2)$$

As we analyze the two-dimensional (2D) projection of the trajectories, we set n = 2. Using the expressions of the effective temperature and viscosity (see SI), the rescaled diffusion coefficient can be explicitly calculated (eqn (S5))[46] and scales for small temperature increment, linearly with ΔT (Fig. S3), as:

$$\frac{D_{eff}^{HBM} - D_0}{D_0} \propto \frac{\Delta T}{T_0}, \qquad (3)$$
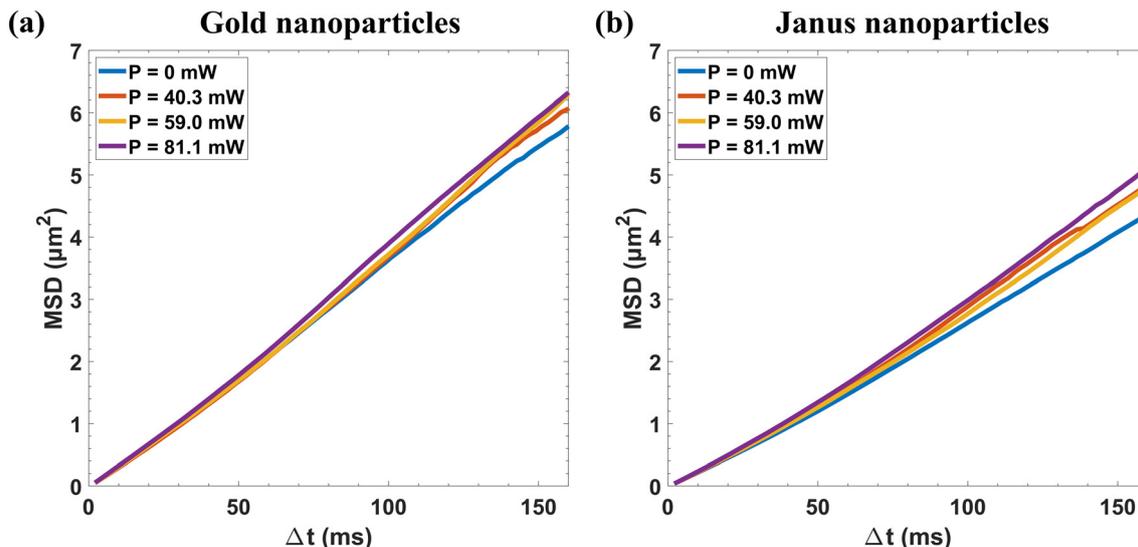
Fig. 8 Ensemble-averaged mean squared displacements (MSDs) for (a) bare gold nanospheres and (b) Janus nanoparticles under increasing optical power. Data represent averages over about 100 individual particles (see Fig. S1 and S2). In both systems, the increasing slopes of the MSD curves with higher illumination intensity indicate enhanced effective diffusion coefficients.

where D_0 is the diffusion coefficient in the absence of laser illumination, $D_0 = k_B T_0/6\pi\eta(T_0)R$. The temperature increase of an isolated plasmonic nanoparticle with absorption cross-section σ_{abs} is given by:[47,48]

$$\Delta T = \frac{\sigma_{abs}P}{2\pi^2\kappa w^2 R} \quad (4)$$

where P is the incident light power, κ the thermal conductivity of the surrounding solvent ($\kappa = 0.6$ W m^{-1} K^{-1} for water), and w the beam waist. For an excitation wavelength of $\lambda = 532$ nm, Mie theory yields an estimation of the absorption cross-section of $\sigma_{abs} \approx 5000$ nm^2 for the Au nanoparticles used in this study. Combining eqn (3) and (4), the contribution arising from hot Brownian motion is thus expected to have a linear dependence with the light intensity for a set of thermally independent particles:

$$\frac{D_{eff}^{HBM} - D_0}{D_0} \propto P. \quad (5)$$

For self-propelling active particles, such as the self-thermophoretic Janus nanoparticles studied here, the MSD acquires an additional contribution to account for the persistent and directed motion, as follows:[49]

$$MSD(\Delta t) = 4D_{eff}^{HBM}\cdot\Delta t + \frac{v^2\tau_R^2}{2}\left[\frac{2\Delta t}{\tau_R} + e^{-2\Delta t/\tau_R} - 1\right], \quad (6)$$

where v is the propulsion speed, and τ_R is the characteristic rotational diffusion time, inversely related to the rotational diffusion coefficient D_R by $\tau_R = D_R^{-1}$.

The MSD behavior depends strongly on the timescale over which particle motion is probed. At long timescales, specifically when $\Delta t \gg \tau_R$, as for our experimental conditions (see below), the MSD expression in eqn (6) reduces to a linear

dependence in time, indicating an effective active diffusive regime:

$$MSD(\Delta t) \approx [4\cdot D_{eff}^{HBM} + v^2\tau_R]\Delta t. \quad (7)$$

This apparent diffusive behavior for active particles arises because rotational diffusion randomizes the propulsion direction over time, transforming persistent motion into a random walk leading to a substantial enhancement of the effective diffusion coefficient over its (hot) Brownian value, namely:[49]

$$D_{eff}^{active} = D_{eff}^{HBM} + \frac{1}{4}v^2\tau_R. \quad (8)$$

This expression captures the enhanced diffusive behavior of active particles at long times combining effects of thermal fluctuations and self-propulsion. On timescales longer than the characteristic rotational diffusion time, the motion resembles that of passive particles (Fig. 7), but with a markedly larger effective diffusion coefficient (eqn (8)).

This long timescale regime applies to our Janus nanoparticles, as the time range accessible in our experiments – determined by the frame rate during video acquisition – is 2.1 ms and above (see Materials and methods). This is nearly one order of magnitude larger than the characteristic rotational time $\tau_R \approx 0.22$ ms (calculated for a spherical particle with a diameter of 66 nm), confirming that $\Delta t \gg \tau_R$.

Thus, for both Janus and bare gold nanoparticles, the MSD is expected to follow a diffusive regime (MSD $\propto \Delta t$) with an effective diffusion coefficient, D_{eff}, differing only by the additional velocity contribution stemming from self-propulsion. Under illumination, the particle speed is expected to scale linearly with the laser power P and hence with the surface temperature increase ΔT (see eqn (4)),[10] leading,

according to eqn (8), to a quadratic dependence of the normalized effective diffusion coefficient,

$$\frac{D_{\text{eff}}^{\text{active}} - D_0}{D_0} \propto a \cdot P + b \cdot P^2 \quad (9)$$

where a and b are two constants associated with hot Brownian motion and self-propulsion, respectively.

The experimental averaged MSDs for both Janus and bare gold nanoparticles are shown in Fig. 8, and linear fits of these curves provide the corresponding effective diffusion coefficients, which are presented in Fig. 9(a). For the samples without optical excitation, the fits yield diffusion coefficients of $D_{0,\text{Au}} = 8.98 \pm 0.25$ μm^2 s^{-1} and $D_{0,\text{Janus}} = 6.49 \pm 0.25$ μm^2 s^{-1} (Fig. S1 and S2). Using the Stokes–Einstein equation, these values correspond to hydrodynamic diameters of $d_{\text{H,Au}} = 54.6 \pm 1.5$ nm and $d_{\text{H,Janus}} = 75.6 \pm 2.9$ nm, respectively. As expected, these hydrodynamic diameters are larger than the bares core sizes d obtained from the size distribution measured by TEM (Fig. 2), and are consistent with $d_{\text{H}} \sim d + \kappa^{-1}$, where $\kappa^{-1} = 13$ nm is the Debye screening length at the experimental ionic strength ($I = 0.5$ mM) used in our nanoparticle suspensions (see Materials and methods).

Characterizing the active behavior of Janus nanoparticles under illumination solely from their MSD is challenging, as it requires precise quantification of the light-induced enhancement in both translational and rotational diffusion (eqn (6) and (8)).[50,51] To isolate the contribution of active motion and disentangle it from hot Brownian motion, we compare the dynamics of the Janus nanoparticles with that of bare gold nanoparticles under identical experimental conditions and

same laser illumination. To account for the size difference caused by the silica shell on the Janus particles, we analyze the rescaled effective translational diffusion coefficient, $(D_{\text{eff}} - D_0)/D_0$, where D_0 is the diffusion coefficient in the absence of laser illumination. This parameter quantifies the relative increase in the effective diffusion coefficient for both systems, as shown in Fig. 9(b). If the observed enhancement was solely due to hot Brownian motion, the increase in diffusion due to internal heating of the Janus particles should not exceed that of the bare gold nanoparticles. However, our results reveal that the relative increase of the normalized effective diffusion coefficient is consistently higher for the Janus nanoparticles than for the bare gold nanoparticles, demonstrating that Janus particles exhibit significant self-propulsion.

The quantitative analysis is provided below. The dependence of Au nanoparticles on light intensity deviates from linearity at the highest laser power, suggesting that collective thermal effects contribute to their heating. When several nanoparticles are illuminated at the same time, the temperature increase experienced by a nanoparticle also stems from neighboring nanoparticles heating their environment.[48] This effect originates from the long-range temperature diffusion profile around a source of heat, decaying as $\Delta T(r) \propto 1/r$, r being the distance from the heat source.[42] As shown in Fig. S4, the temperature increase calculated from the experimental rescaled diffusion coefficient (Fig. 9(b)) using the HBM theory (eqn (S5) and Fig. S3) consistently exceeds the prediction of eqn (4) for thermally independent particles. This discrepancy persists even when considering the lower limit of the beam size, which corresponds to the upper limit of the laser power density (Fig. S4).
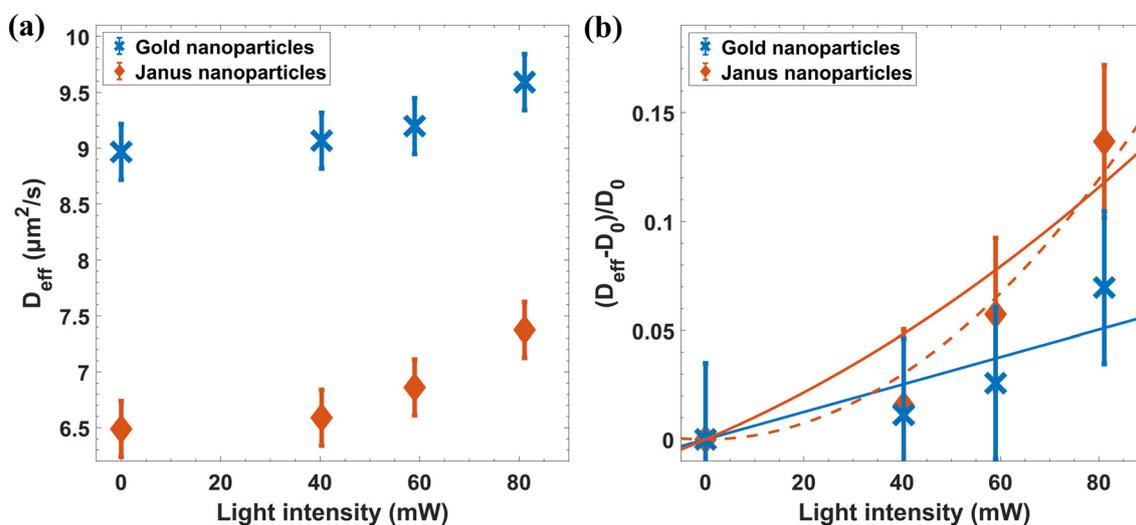

Fig. 9 Experimental evidence of self-thermophoretic motion for Janus nanoparticles under optical illumination. (a) Effective diffusive coefficients extracted from MSD analysis increase with light intensity. The lower absolute diffusion values of Janus nanoparticles, compared to bare Au particles, stem from their larger size due to the silica shell. (b) Normalized effective diffusion coefficients as a function of laser intensity. D_0 is the diffusion coefficient in absence of illumination. The enhanced dynamics of Janus nanoparticles reveal light-activated self-propulsion in addition to hot Brownian motion, which is also observed for Au nanoparticles (linear fit (eqn (5)) shown as a blue line). Orange lines represent quadratic fits for Janus nanoparticles: the dashed curve is purely quadratic (eqn (9), $a = 0$), while the solid curve includes the same linear contribution as for Au nanobeads (eqn (9), $a = 6.35 \times 10^{-4}$, $b = 9.85 \times 10^{-6}$). Error bars represent estimated experimental uncertainties.

Conversely, for Janus nanoparticles, a non-linear dependence of the normalized effective diffusion coefficient on laser power is expected from eqn (9), in agreement with the experimental results shown in Fig. 9(b). To isolate the contribution of active motion, we have used in eqn (9) the same fitting parameter accounting for HBM as that determined for bare gold nanoparticles (namely parameter a), while allowing the active term b to vary freely. Although the fit quality remains limited, the pronounced increase in the normalized effective diffusion coefficient provides conclusive evidence of an additional contribution from self-thermophoresis-induced motion to the dynamics of Janus nanoparticles. At the highest illumination, active motion accounts for approximately 50% of the total diffusion enhancement. The corresponding propulsion speed of the Janus particles can then be estimated using eqn (8), assuming $\tau_R = D_R^{-1}(T_{eff}) \approx D_R^{-1}(T_0)$, which yields $v \sim 35$ μm s^{-1}. The corresponding Péclet number can also be calculated and gives Pe ≈ 0.3, confirming *a posteriori* that the system operates in a regime where active and passive Brownian contributions are comparable.

Conclusion

In summary, we have successfully produced stable nanoscale gold–silica Janus particles and demonstrated their self-thermophoretic propulsion under optical illumination. Using single particle tracking, we resolved individual particle trajectories, and determined effective diffusion coefficients by analyzing the mean squared displacements of approximately one hundred individual traces per experimental condition, ensuring statistical relevance. The limited amplitude of the active contribution within the explored irradiation power range, combined with the intrinsic passive hot Brownian diffusion of the nanoparticles, results in an experimental system at low Péclet number in which active and passive contributions to particle dynamics are comparable in magnitude. In this low Péclet regime, our results reveal that the Janus particles exhibit a systematically and significantly higher relative increase in normalized effective diffusivity compared to bare gold nanobeads under identical illumination conditions. This enhancement, which accounts up to about 50% of the total dynamics, provides direct experimental evidence of visible-light-induced active motion in Janus nanoparticles. Furthermore, since the active behavior is both optically controlled and reversible, our system represents a simple, fuel-free, tunable platform for studying active matter and non-equilibrium dynamics at the nanoscale.

Author contributions

H. T. performed the experiments, acquired and analyzed the data, and wrote the first version of the manuscript. C. M. and B. A. synthesized the nanoparticles. L. B. and H. T. developed and assembled the optical setup. E. G. conceived and supervised the project, analyzed and interpreted the data, secured funding, wrote and edited the manuscript. All authors reviewed and approved the final version of the manuscript.

Conflicts of interest

There are no conflicts to declare.

Data availability

All the data supporting the findings of this study are included in the article and its supplementary information (SI) and will be made available on request.

Supplementary information: detailed dynamics analysis comprising mean squared displacement (MSD) curves for all individual trajectories of both Au and Au–SiO$_2$ nanoparticle systems under each experimental condition, the theoretical expressions and plot of the normalized diffusion coefficient and viscosity for hot Brownian motion, as well as the corresponding temperature increase as a function of laser illumination. A dark-field microscopy movie of Janus nanoparticles in absence of laser illumination is provided (AVI). See DOI: https://doi.org/10.1039/d5nr04182a.

References

1 J. Schwarz-Linek, J. Arlt, A. Jepson, A. Dawson, T. Vissers, D. Miroli, T. Pilizota, V. A. Martinez and W. C. K. Poon, Escherichia coli as a model active colloid: A practical introduction, *Colloids Surf., B*, 2016, **137**, 2–16.

2 H. H. Wensink, J. Dunkel, S. Heidenreich, K. Drescher, R. E. Goldstein, H. Löwen and J. M. Yeomans, Meso-scale turbulence in living fluids, *Proc. Natl. Acad. Sci. U. S. A.*, 2012, **109**, 14308–14313.

3 F. Jülicher, K. Kruse, J. Prost and J. F. Joanny, Active behavior of the Cytoskeleton, *Phys. Rep.*, 2007, **449**, 3–28.

4 N. Kodera, D. Yamamoto, R. Ishikawa and T. Ando, Video imaging of walking myosin V by high-speed atomic force microscopy, *Nature*, 2010, **468**, 72–76.

5 T. Sanchez, D. T. N. Chen, S. J. DeCamp, M. Heymann and Z. Dogic, Spontaneous motion in hierarchically assembled active matter, *Nature*, 2012, **491**, 431–434.

6 A. Ghosh and P. Fischer, Controlled Propulsion of Artificial Magnetic Nanostructured Propellers, *Nano Lett.*, 2009, **9**, 2243–2245.

7 I. Buttinoni, G. Volpe, F. Kümmel, G. Volpe and C. Bechinger, Active Brownian motion tunable by light, *J. Phys.: Condens. Matter*, 2012, **24**, 284129.

8 H. R. Vutukuri, M. Lisicki, E. Lauga and J. Vermant, Light-switchable propulsion of active particles with reversible interactions, *Nat. Commun.*, 2020, **11**, 2628.

9 T. He, Y. Yang and X.-B. Chen, Propulsion mechanisms of micro/nanorobots: a review, *Nanoscale*, 2024, **16**, 12696–12734.

10 H.-R. Jiang, N. Yoshinaga and M. Sano, Active Motion of a Janus Particle by Self-Thermophoresis in a Defocused Laser Beam, *Phys. Rev. Lett.*, 2010, **105**, 268302.

11 T.-C. Lee, M. Alarcón-Correa, C. Miksch, K. Hahn, J. G. Gibbs and P. Fischer, Self-Propelling Nanomotors in the Presence of Strong Brownian Forces, *Nano Lett.*, 2014, **14**, 2407–2412.

12 A. Christoulaki and E. Buhler, Light-induced directed self-propulsion of active nanosized particles in a three-dimensional Brownian environment probed by heterodyne photon correlation laser spectroscopy, *Phys. Rev. E*, 2025, **111**, 015433.

13 C. Bechinger, R. Di Leonardo, H. Löwen, C. Reichhardt, G. Volpe and G. Volpe, Active particles in complex and crowded environments, *Rev. Mod. Phys.*, 2016, **88**, 045006.

14 J. Wang and W. Gao, Nano/Microscale Motors: Biomedical Opportunities and Challenges, *ACS Nano*, 2012, **6**, 5745–5751.

15 D. Patra, S. Sengupta, W. Duan, H. Zhang, R. Pavlick and A. Sen, Intelligent, self-powered, drug delivery systems, *Nanoscale*, 2013, **5**, 1273–1283.

16 B. J. Nelson, I. K. Kaliakatsos and J. J. Abbott, Microrobots for Minimally Invasive Medicine, *Annu. Rev. Biomed. Eng.*, 2010, **12**, 55–85.

17 W. Gao and J. Wang, The Environmental Impact of Micro/Nanomachines: A Review, *ACS Nano*, 2014, **8**, 3170–3180.

18 S. J. Ebbens, Active colloids: Progress and challenges towards realising autonomous applications, *Curr. Opin. Colloid Interface Sci.*, 2016, **21**, 14–23.

19 L. K. E. A. Abdelmohsen, F. Peng, Y. Tu and D. A. Wilson, Micro- and nano-motors for biomedical applications, *J. Mater. Chem. B*, 2014, **2**, 2395–2408.

20 C. M. Maier, M. A. Huergo, S. Milosevic, C. Pernpeintner, M. Li, D. P. Singh, D. Walker, P. Fischer, J. Feldmann and T. Lohmüller, Optical and Thermophoretic Control of Janus Nanopen Injection into Living Cells, *Nano Lett.*, 2018, **18**, 7935–7941.

21 H. Su, S. Li, G.-Z. Yang and K. Qian, Janus Micro/Nanorobots in Biomedical Applications, *Adv. Healthcare Mater.*, 2023, **12**, 2202391.

22 N. Ruiz-González, D. Esporrín-Ubieto, I.-D. Kim, J. Wang and S. Sánchez, Micro- and Nanomotors: Engineered Tools for Targeted and Efficient Biomedicine, *ACS Nano*, 2025, **19**, 8411–8432.

23 X. Lin, T. Si, Z. Wu and Q. He, Self-thermophoretic motion of controlled assembled micro-/nanomotors, *Phys. Chem. Chem. Phys.*, 2017, **19**, 23606–23613.

24 S. Palagi, D. P. Singh and P. Fischer, Light-Controlled Micromotors and Soft Microrobots, *Adv. Opt. Mater.*, 2019, **7**, 1900370.

25 H. Šípová-Jungová, D. Andrén, S. Jones and M. Käll, Nanoscale Inorganic Motors Driven by Light: Principles, Realizations, and Opportunities, *Chem. Rev.*, 2020, **120**, 269–287.

26 C. Calero, E. L. Sibert III and R. Rey, Self-thermophoresis at the nanoscale using light induced solvation dynamics, *Nanoscale*, 2020, **12**, 7557–7562.

27 S. Liu, L. Lin and H.-B. Sun, Opto-Thermophoretic Manipulation, *ACS Nano*, 2021, **15**, 5925–5943.

28 F. Schmidt, H. Šípová-Jungová, M. Käll, A. Würger and G. Volpe, Non-equilibrium properties of an active nanoparticle in a harmonic potential, *Nat. Commun.*, 2021, **12**, 1902.

29 P. S. Kollipara, Z. Chen and Y. Zheng, Optical Manipulation Heats up: Present and Future of Optothermal Manipulation, *ACS Nano*, 2023, **17**, 7051–7063.

30 M. Rey, G. Volpe and G. Volpe, Light, Matter, Action: Shining Light on Active Matter, *ACS Photonics*, 2023, **10**, 1188–1201.

31 D. Bronte Ciriza, A. Callegari, M. G. Donato, B. Çiçek, A. Magazzù, I. Kasianiuk, D. Kasyanyuk, F. Schmidt, A. Foti, P. G. Gucciardi, G. Volpe, M. Lanza, L. Biancofiore and O. M. Maragò, Optically Driven Janus Microengine with Full Orbital Motion Control, *ACS Photonics*, 2023, **10**, 3223–3232.

32 F. Braun, M. F. P. Wagner, M. E. Toimil-Molares and R. von Klitzing, Comparison of Different Preparation Techniques of Thermophoretic Swimmers and Their Propulsion Velocity, *Langmuir*, 2024, **40**, 5606–5616.

33 L. He, T. He, Y. Yang and X.-B. Chen, Material selection, preparation, driving and applications of light-driven micro/nano motors: a review, *Nanoscale*, 2025, **17**, 11894–11933.

34 N. Castro, D. Constantin, P. Davidson and B. Abecassis, Solution self-assembly of plasmonic Janus nanoparticles, *Soft Matter*, 2016, **12**, 9666–9673.

35 N. G. Bastús, J. Comenge and V. Puntes, Kinetically Controlled Seeded Growth Synthesis of Citrate-Stabilized Gold Nanoparticles of up to 200 nm: Size Focusing versus Ostwald Ripening, *Langmuir*, 2011, **27**, 11098–11105.

36 T. Chen, G. Chen, S. Xing, T. Wu and H. Chen, Scalable Routes to Janus Au-SiO$_2$ and Ternary Ag-Au-SiO$_2$ Nanoparticles, *Chem. Mater.*, 2010, **22**, 3826–3828.

37 V. Amendola, R. Pilot, M. Frasconi, O. M. Maragò and M. A. Iatì, Surface plasmon resonance in gold nanoparticles: a review, *J. Phys.: Condens. Matter*, 2017, **29**, 203002.

38 J. C. Crocker and D. G. Grier, Methods of Digital Video Microscopy for Colloidal Studies, *J. Colloid Interface Sci.*, 1996, **179**, 298–310.

39 H. Shen, L. J. Tauzin, R. Baiyasi, W. Wang, N. Moringo, B. Shuang and C. F. Landes, Single Particle Tracking: From Theory to Biophysical Applications, *Chem. Rev.*, 2017, **117**, 7331–7376.

40 F. Novotný and M. Pumera, Nanomotor tracking experiments at the edge of reproducibility, *Sci. Rep.*, 2019, **9**, 13222.

41 W. Wang and T. E. Mallouk, A Practical Guide to Analyzing and Reporting the Movement of Nanoscale Swimmers, *ACS Nano*, 2021, **15**, 15446–15460.

42 D. Rings, R. Schachoff, M. Selmke, F. Cichos and K. Kroy, Hot Brownian Motion, *Phys. Rev. Lett.*, 2010, **105**, 090604.

43 K. Kroy, D. Chakraborty and F. Cichos, Hot microswimmers, *Eur. Phys. J.: Spec. Top.*, 2016, **225**, 2207–2225.

44 L. F. Guerra, T. W. Muir and H. Yang, Temperature-Dependent Translation-Rotation Diffusivity Divergence in Hot Brownian Motion Directly Observed by Single-Particle T-Jump Tracking, *J. Phys. Chem. C*, 2025, **129**, 2083–2089.

45 D. Rings, D. Chakraborty and K. Kroy, Rotational hot Brownian motion, *New J. Phys.*, 2012, **14**, 053012.

46 D. Rings, M. Selmke, F. Cichos and K. Kroy, Theory of Hot Brownian Motion, *Soft Matter*, 2011, **7**, 3441–3452.

47 G. Baffou, R. Quidant and F. J. García de Abajo, Nanoscale Control of Optical Heating in Complex Plasmonic Systems, *ACS Nano*, 2010, **4**, 709–716.

48 G. Baffou, F. Cichos and R. Quidant, Applications and challenges of thermoplasmonics, *Nat. Mater.*, 2020, **19**, 946–958.

49 J. R. Howse, R. A. L. Jones, A. J. Ryan, T. Gough, R. Vafabakhsh and R. Golestanian, Self-Motile Colloidal Particles: From Directed Propulsion to Random Walk, *Phys. Rev. Lett.*, 2007, **99**, 048102.

50 M. Xuan, Z. Wu, J. Shao, L. Dai, T. Si and Q. He, Near Infrared Light-Powered Janus Mesoporous Silica Nanoparticle Motors, *J. Am. Chem. Soc.*, 2016, **138**, 6492–6497.

51 M. R. Bailey, A. R. Sprenger, F. Grillo, H. Löwen and L. Isa, Fitting an active Brownian particle's mean-squared displacement with improved parameter estimation, *Phys. Rev. E*, 2022, **106**, L052602.